Bull Math Biol
https://doi.org/10.1007/s11538-018-0441-3

Society for Mathematical Biology

ORIGINAL ARTICLE

Predictive Modeling of Neuroblastoma Growth Dynamics in Xenograft Model After Bevacizumab Anti-VEGF Therapy

Yixuan He[1,2] · **Anita Kodali**[1] · **Dorothy I. Wallace**[1]

Received: 4 August 2017 / Accepted: 27 April 2018

Abstract Neuroblastoma is the leading cause of cancer death in young children. Although treatment for neuroblastoma has improved, the 5-year survival rate of patients still remains less than half. Recent studies have indicated that bevacizumab, an anti-VEGF drug used in treatment of several other cancer types, may be effective for treating neuroblastoma as well. However, its effect on neuroblastoma has not been well characterized. While traditional experiments are costly and time-consuming, mathematical models are capable of simulating complex systems quickly and inexpensively. In this study, we present a model of vascular tumor growth of neuroblastoma IMR-32 that is complex enough to replicate experimental data across a range of tumor cell properties measured in a suite of in vitro and in vivo experiments. The model provides quantitative insight into tumor vasculature, predicting a linear relationship between vasculature and tumor volume. The tumor growth model was coupled with known pharmacokinetics and pharmacodynamics of the VEGF blocker bevacizumab to study its effect on neuroblastoma growth dynamics. The results of our model suggest that total administered bevacizumab concentration per week, as opposed to dosage regimen, is the major determining factor in tumor suppression. Our model also establishes an exponentially decreasing relationship between administered bevacizumab concentration and tumor growth rate.

Electronic supplementary material The online version of this article (https://doi.org/10.1007/s11538-018-0441-3) contains supplementary material, which is available to authorized users.

✉ Yixuan He
yixuan.he.18@dartmouth.edu

[1] Department of Mathematics, Dartmouth College, 1145 Hinman, Hanover, NH 03755-3551, USA

[2] Department of Biological Sciences, Dartmouth College, Hanover, NH 03755, USA

Published online: 14 June 2018

Keywords Cancer modeling · Neuroblastoma · Mathematical model · VEGF · Tumor growth

1 Introduction

According to the Center for Disease Control, cancer is the second leading cause of death in the USA (U.S. Cancer Statistics Working 2017). Mathematics can provide significant contributions to experimental cancer investigation as it is a powerful tool to test hypotheses, confirm experiments, and predict likely outcomes across a range of treatment options. Mathematical models are capable of simulating complex systems quickly without the enormous costs of laboratory experiments and clinical trials necessary in the traditional drug discovery process. This allows researchers to gain a better understanding of cancer growth dynamics and to design better treatment strategies to improve the quality of lives of the over one million people diagnosed with cancer each year.

Neuroblastoma, a rapidly dividing and highly vascularized cancer, is the leading cause of cancer death in young children. It is the most common type of solid cancer diagnosed in children younger than a year old, with about 700 new cases diagnosed each year in the USA (Segerström et al. 2006). Although treatment for neuroblastoma has improved, the 5-year survival rate of patients with high-risk neuroblastoma still remains less than 40% (Segerström et al. 2006), despite aggressive treatment protocols involving high-dose chemotherapy, total body irradiation, and bone marrow transplants.

It is well established that tumor growth in vivo exists in two main phases: an avasculature and a vasculature phase (Tang et al. 2014). In the avasculature phase, the tumor does not have its own blood supply and is relatively harmless. Upon secretion of tumor angiogenic factors (TAFs), tumors can establish independent blood supply by inducing neighboring blood vessels to growth toward the tumor. This new formation of blood vessels to supply nutrients and/or metabolites to starving tissue is called angiogenesis (Alarcon et al. 2005). With access to endless nutrients, the now vascularized tumor cells can metastasize, rendering them potentially lethal (Alarcon et al. 2005; Tang et al. 2014).

In our model, we focus on one TAF highly expressed in tumors—vascular endothelial growth factor (VEGF) and a drug which inhibits its production. VEGF and VEGF receptors have been the target of extensive research in the development of cancer therapeutic agents to hinder tumor angiogenesis and growth. Most notably, bevacizumab (Avastin®; a humanized anti-VEGF-A antibody) was the first angiogenesis inhibitor proven to be effective in prolonging survival and delaying tumor progression in patients with various cancers. In fact, bevacizumab has been approved by the FDA and is commonly used in the treatment of metastatic colorectal cancer, non-small cell lung cancer metastatic renal cell carcinoma, metastatic breast cancer, and epithelial ovarian cancer (Keating 2014). Recent studies have indicated that bevacizumab may be effective in neuroblastoma treatment as well (Segerström et al. 2006; Sims et al. 2008).

Many models exist for cancer growth, ranging from extremely complex to simple with an enormous range in between. Simple models often only attempt to match

total tumor size (Demidenko 2006; Marušić et al. 1994), but complex models, while able to replicate a wide range of experimental data, frequently require knowledge of many specific parameters, some of which are difficult to obtain (Landry et al. 1982; Piantadosi 1985). Many of these models attempt to capture a key characteristic of tumor in vivo growth—angiogenesis and vascularization.

In this study, we extend a model adapted from Wallace et al., since it includes signaling mechanisms known to control pre-vascular tumor growth (Wallace et al. 2016). Tumor cell lines grown as in vitro spheroids are known to cease growth. This phenomenon was originally conjectured to be due to the limits of diffusion of nutrients (Folkman and Hochberg 1973). However, this hypothesis does not stand up to scrutiny. Diffusion limits do not rule out the existence of large spheroids with a small outer layer of proliferating cells, thin enough to receive nutrients. Numerical experiments confirm that diffusion of nutrients alone is insufficient to explain cessation of growth (Menchón and Condat 2008, 2009). Consistent with the numerical experiments, imaging techniques confirm that mature spheroids have a necrotic core and thin rim of proliferating cells (Sherar et al. 1987; Folkman and Hochberg 1973). Yet, most models of tumor growth attempt to limit pre-vascular growth with a logistic or Gompertz term, assuming that access to nutrients is equal for all cells, that all cells are actively proliferating, and that some natural limit to growth exists (Hahnfeldt et al. 1999; Byrne 2010; Alarcón et al. 2006). The model presented by Wallace et al. avoids this assumption by incorporating a known mediator of pre-vascular tumor growth, tumor necrosis factor (TNF) (Wallace et al. 2016). Experiments show that the necrotic core produces tumor necrosis factors that inhibit proliferation (Freyer 1988). A specific factor, known as TNF-alpha, has been shown to induce apoptosis in actively proliferating cells (Botchkina et al. 1997; Leeuwenberg et al. 1995). Even simple models that use tumor necrosis factor to limit growth will produce in silico spheroids with qualitatively correct development (Wallace and Guo 2013).

Six recent papers model the use of VEGF blocking drugs on tumors (De Mattei et al. 2016; Mollard et al. 2017; Pinho et al. 2013; Argyri et al. 2016; Poleszczuk et al. 2015; Lignet et al. 2013). Of these, four use the logistic or Gompertz model to limit pre-vascular growth, adjusting the limit to account for increasing vasculature (Mollard et al. 2017; Pinho et al. 2013; Argyri et al. 2016; Poleszczuk et al. 2015). The remaining two include compartments for hypoxic cells that are known to produce the VEGF signal, but do not include necrotic cells or the TNF-alpha produced by these which are the only known mechanisms of pre-vascular growth control, nor do they include a particular data set (De Mattei et al. 2016; Lignet et al. 2013). Three of these studies model bevacizumab specifically (Mollard et al. 2017; Argyri et al. 2016; Poleszczuk et al. 2015) but none of these uses the specific two-compartment pharmacokinetics and pharmacodynamics for this drug as we do here (Lu et al. 2008a, b; Wu et al. 2012).

In this study, we present a multiscale mathematical model of vascular tumor growth of neuroblastoma IMR-32 with and without treatment that addresses the issues described above. The model is complex enough to replicate experimental data on a range of tumor properties in vivo, including monolayer, spheroid, and xenograft studies, while restraining the number of parameters in the system of differential equations to the number of measured quantities. In addition, our model is able to provide quanti-

tative insight into tumor vasculature. Various treatments regimens of bevacizumab are implemented to determine its effect on neuroblastoma growth dynamics. Our model provides a better understanding of neuroblastoma development in vivo as well as bevacizumab pharmacodynamics. The resulting parameterized model can be used to facilitate the design of optimal treatment strategies for neuroblastoma patients.

2 Methods

Cancer cell lines that have the capacity to form solid tumors can be cultured, studied, and experimented upon in three modalities outside the human body: in vitro monolayer, 3-D spheroid cultures, and in vivo mouse xenograft models. Monolayer in vitro cultures represent unfettered growth of cells in the presence of abundant nutrient, with cell growth characterized as exponential. Three-dimensional in vitro spheroid cultures result in a growing ball of cells that develop a tripartite structure with a central necrotic core, an actively proliferating rim, and an intermediate zone of hypoxic quiescent cells (Folkman et al. 1966). While spheroids have been shown to be a good representation of pre-angiogenesis in vivo tumors (Kim 2005; Edmondson et al. 2014), xenograft experiments in vivo are the most similar to human tumors as they include the growth of vasculature, are derived from human cancer cell lines, and are grown in mice.

A tumor cell can be grown as a monolayer, 3-D spheroid, or xenograft culture. Thus, a model for cancer should have the capability of describing growth in all three scenarios. In this paper, we build such a model for the growth of neuroblastoma IMR-32 grown as in vitro monolayer, spheroids, and in vivo solid vascularized tumors. The model must include, at minimum, compartments corresponding to rapidly proliferating cells in various stages of the cell cycle, quiescent and necrotic cells, growing vasculature, and the presence of signaling compounds. Models of treatment would include pharmacokinetic components specific to the anti-VEGF drug bevacizumab. Furthermore, it should replicate multiple experimental results on three scales. In particular:

1. Preventing the transition from proliferating to quiescent compartments should result in exponential growth that matches monolayer data. The volume of cells in this model would grow exponentially.
2. Allowing transitions from proliferating to quiescent compartments but preventing vascular growth should result in a spheroid that matches qualitative observations of spheroid growth, in particular, the cessation of tumor growth with the continued presence of necrotic, quiescent, and actively proliferating cells (Folkman and Hochberg 1973).
3. The full model with angiogenesis should match xenograft data. The full model of untreated xenograft would grow linearly after an initial period, as observed for most tumors (Brú et al. 2003).

2.1 Model Overview

The model we consider tracks ten quantities. Three of these (G_1, S, G_2) are measured cell cycle compartments of the population of rapidly proliferating tumor cells

($P = G_1, + S + G_2$). The sub-model containing only these components grows exponentially and may be fit to monolayer experiments for the cell line, using the methods described in Wallace et al. (2016).

When placed in an in vitro test tube culture, IMR-32 cells form spheroids. These have an outer shell of proliferating cells (P), an inner shell of quiescent, non-proliferating cells (Q), and a necrotic core (N) (Sherar et al. 1987; Folkman et al. 1966). Spheroids are known to cease growth at a predictable size while maintaining a thin shell of proliferating cells (Folkman et al. 1966), and it has been shown that diffusive limits are inadequate to explain this cessation of growth (Menchón and Condat 2009). However, it is also now known that substances produced by the necrotic cells, generally called tumor necrosis factors (TNF's), cause growth to stop (Freyer 1988). One particular factor, called TNF-α, binds to the p-75 receptor of proliferating cells and causes apoptosis. It has been observed that the signal is produced as a by-product of necrosis and is responsible for cessation of spheroid growth in the absence of increasing vasculature (Shweiki et al. 1992; Szlosarek and Balkwill 2003). In our model, TNF-α is produced by necrotic cells at a rate of $c_f A(s_R + A)^{-1}$ and is assumed to affect the proliferating cells at any stage in the proliferating compartment via apoptosis. The concentration of TNF-α (A) is tracked in this model. The spheroid sub-model is similar to the one in Wallace with nutrient availability modeled in the presence of constant supply rather than in proportion to spheroid surface area (Wallace et al. 2016). It consists only of a few compartments (G_1, S, G_2, Q, N, A) and models a spheroid that ceases growth. The spheroid sub-model reproduces both the qualitative behavior described in Folkman et al. and the quantitative measurements in Carlsson et al. (1983). As it is fully described in Wallace et al. (2016), we will only summarize the main features here.

When hypoxic or in the presence of TNF-α, cells may produce the tumor angiogenesis factor VEGF to cause vasculature to grow (Jing et al. 2011; Sasi et al. 2012). Each cell line does this to a different extent, and different types of tumors vascularize differently. The VEGF signal itself is represented in the model as R. Thus, VEGF, represented by R, is assumed to be related to cells of all three states of the tumor: the proliferating compartments ($G_2 + S + G_2$), the necrotic compartment (N), and the hypoxic quiescent compartment (Q). The production rates of VEGF are not well documented; thus, the spheroid sub-model was tuned to produce the VEGF concentrations observed in Takagi et al., without altering the parameters already computed for the spheroid sub-model (Takagi et al. 2007).

Xenograft culture in vivo differs from multicellular spheroid mainly in their ability to grow vasculature in a process known as angiogenesis. Vasculature (V) is grown proportionally to VEGF signaling (R) produced by hypoxic quiescent cells (Q) or by proliferating cells in response to TNF-alpha. The rate at which P and R control growth of vasculature is controlled by parameters associated to vascular growth and its sensitivity to the signal (R), as well as the ability of vasculature to deliver nutrient to the tumor cells. In addition, few parameters derived for the spheroid are dependent on external conditions in which the spheroid grows, and these may be different for xenograft culture. The fully vascularized control (untreated) xenograft model was tuned to data from several experimental systems by Segerstrom et al. and Ackerman et al. without altering parameters intrinsic to the spheroid sub-model (Segerström et al.

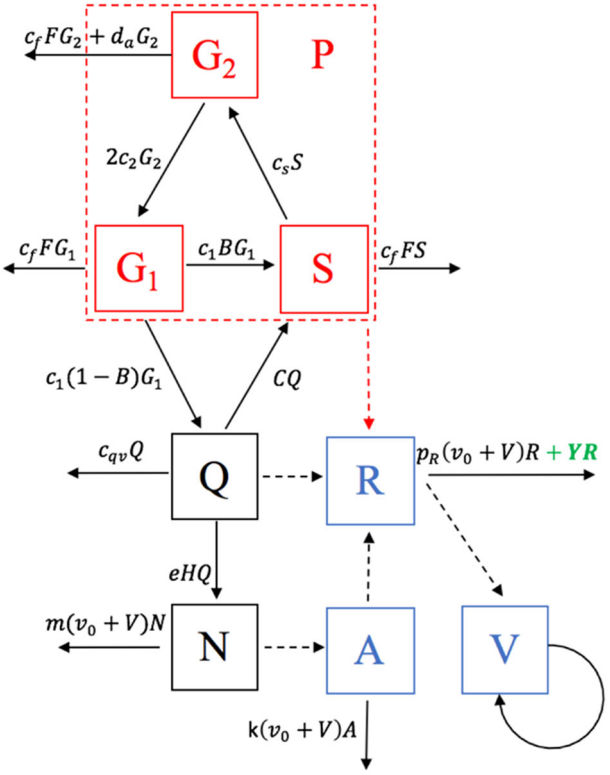

Fig. 1 Compartmental model for the full system. Red boxes model monolayer culture. Red and black boxes model spheroid culture. Solid arrows represent cell transitions. Dashed arrows reflect influence of one compartment on another. Symbols in green represent treatment response to bevacizumab. Each system can be reduced to a smaller one by setting one or more parameters or initial conditions equal to zero (Color figure online)

2006; Ackermann et al. 2011). The control xenograft model exhibits long-term linear growth.

The full model of the treated tumor includes the drug kinetics of bevacizumab which can be described by a two-compartment model (E, X) developed by Wu et al. (2012). Bevacizumab is a VEGF blocker that binds to the VEGF signal (R), thereby removing some R from the system. Wu et al. also describe a functional form for the pharmacodynamics they observed, but did not include the VEGF signal (R) explicitly in their model. We have reworked the pharmacodynamics to reflect this change and refitted parameters to data from Segerström et al. (2006). No parameters derived for the control xenograft model were altered. The treated xenograft model shows continued linear growth at a reduced rate compared to the control xenograft model, just as the data does. The compartment model is illustrated in Fig. 1.

2.2 Model Equations

The full set of differential equations is given by:

$$G_1^{'} = 2c_2G_2 - c_1\,(B)\,G_1 - c_1\,(1-B)\,G_1 - c_f F G_1 \tag{1}$$

= cell division − passage to S − passage to Q − apoptosis due to TNF-α.

Here, B is the percent of cells that are not hypoxic, while $(1-B)$ is the remaining percent that are hypoxic. Setting $B = 1$ gives monolayer growth patterns.

$$S' = c_1 B G_1 - c_s S + C Q - c_f F S \tag{2}$$

= passage from G_1 − passage to G_2 + return of cells from Q − apoptosis due to TNF-α

$$G_2^{'} = c_s S - c_2 G_2 - d_a G_2 - c_f F G_2 \tag{3}$$

= passage from S − cell division and passage to G_1 − natural cell apoptosis − apoptosis due to TNF-α

$$Q' = c_1\,(1-B)\,G_1 - C Q - eHQ \tag{4}$$

= passage of hypoxic cells from G_1 − return of cells to S − necrotic death of Q

$$N' = eHQ - m\,(v_0 + V)\,N \tag{5}$$

= necrotic death of Q − natural removal of dead matter

$$A' = jN - k\,(v_0 + V)\,A \tag{6}$$

= production of TNF-α from necrotic tissue − removal of A

$$R' = c_R\,(G_2 + S + G_1)\,\frac{A}{s_R + A} + c_{qv} Q - q_R\,(v_0 + V)\,R - YR \tag{7}$$

= production of VEGF by proliferating cells in the presence of TNF-α + production of VEGF by hypoxic cells − natural removal of signal − removal of signal with therapy

$$V' = c_v \frac{R\,(v_0 + V)}{s_v + R + v_0 + V} \tag{8}$$

= growth of vasculature in the presence of VEGF signal R

$$E' = k_{21}X - k_{10}E - k_{12}E \tag{9}$$

= return of therapy to the primary compartment (blood) from the secondary compartment − first-order removal of drug from system − uptake by secondary compartment

$$X' = k_{12}E - k_{21}X \tag{10}$$

= uptake by secondary compartment − return of therapy to the primary compartment

In the spheroid model, the functional response B, which describes the fraction of cells in G_1 entering Q, is given in relation to available nutrient, taken to be a constant, v_0. In the xenograft model, the fraction, B, is determined by availability of nutrient, $(v_0 + V)$, relative to the volume of cells in G_1. This dynamic is modeled with the Hill function:

$$B = \frac{(v_o + V)}{s_1 + G_1 + v_0 + V} \tag{11}$$

Note that the fraction B rises to 1 as the ratio of V to G_1 rises.

Similarly, the spheroid model gives functional response C, the fraction of quiescent cells that return to proliferating cells in the S phase, in relation to available nutrient, v_0. In the xenograft model, total tumor size is replaced with availability of nutrient to better represent the process of vascularization. The dynamic is modeled with the Hill function:

$$C = c_q \frac{v_0 + c_{qs}V}{s_q + P + v_0 + c_{qs}V} \tag{12}$$

where P is the sum of proliferating compartments.

Under conditions of decreased vasculature and hypoxia, quiescent cells become necrotic (Wallace and Guo 2013). We, thus, introduce the Hill function, H, in the xenograft model to describe this progression from Q to N in terms of vasculature:

$$H = 1 - \frac{V}{s_h + f_h P + g_h Q + V} \tag{13}$$

As vasculature increases, hypoxia decreases and the rate $1 - \mathrm{H}$ drops to zero, stopping necrosis. When vasculature (V) is zero, the same proportion becomes necrotic as in the spheroid model. Constants f_h and g_h were introduced to account for the different nutrient uptake rates by actively proliferating versus quiescent cells.

It is assumed that the effect of TNF-alpha on the proliferating cells can occur at any stage in the proliferating compartment via apoptosis. This occurs through the functional response F at a rate controlled by the transition rate c_f. The dynamic is modeled with the Hill function:

$$F = \frac{A}{s_n + A} \tag{14}$$

Finally, the effect of the anti-VEGF drug, bevacizumab, is represented by the relative rate Y in our model and is given by the Hill function:

$$Y = \frac{c_y\,(v_0 + V)\,E}{s_y + v_0 + V} \tag{15}$$

2.3 Model Parameterization

Using the methods described by Wallace, the monolayer sub-model equations from above (Eqs. 1–3) were first tuned to fit neuroblastoma IMR-32 growth as a monolayer based on data from Seeger et al. (doubling time = 26 h) and Kumar et al. (cell cycle analysis: $g_1* = 0.6008$, $s* = 0.1845$, $g_2* = 0.1925$) (Seeger et al. 1977; Kumar et al. 2014). Cell proportion distribution was maintained but adjusted such that the sum added to 100%. The death rate was fit to a study by Kumar et al. reporting that five percent of cells were apoptotic after 2 days (Kumar et al. 2014). The remaining parameters in the spheroid sub-model were tuned to data from Carlsson et al. (1983). Initial starting conditions were set by dividing the initial tumor size into the proliferating compartments according to percentages reported in Kumar et al. The tumor was assumed to be composed initially of only actively dividing cells, thus initial quantities of N and Q are set to zero.

Vasculature depends on the VEGF signal R and is assumed to have an upper limit. It is given by a Hill function with maximum rate c_v and half saturation s_v. The constant c_v is related to maximum growth rate of endothelial cells. Here, we use a maximal daily growth rate of $\ln(2)/1 = 0.69$ as reported by Tan et al. (2004). Recall that when c_v is set to zero, no growth of vasculature occurs, and the model is reduced to that of an in vitro spheroid model.

To parameterize the production of TNF-α, constants j and k are chosen arbitrarily since they occur only in this single expression. The units of A are arbitrary; scaling A by any constant only affects growth through the function F, which can be offset by scaling s_n by the same factor. By choosing $j = 1$ and $k = j/v_o$, the parameterization problem is reduced to only a choice of s_n. This reduction gives $A* = N*$ at equilibrium. Constants c_f and s_n determine the rate at which the proliferating cells die via apoptosis in response to the signal A.

Remaining parameters in the full xenograft model were tuned to data from xenograft experiments in Ackerman et al. (2011) and Segerstrom et al. (2006). With the exception of three parameters, v_0, c_v, and c_q, all constants from the spheroid model remained the same in the xenograft model. The five remaining parameters, c_{qs}, s_v, s_h, f_h, and g_h, were tuned to best fit the total tumor size based on the control (untreated) runs in several experimental systems by Segerstrom et al. and Ackerman et al. Though Segerstrom et al. did not specify the number of cells initially inoculated into the mice, Ackerman described that they started out by inoculating 1.5×10^7 IMR-32 cells subcutaneously in the nude mice. Previous research indicates that single neuroblastoma cells have an average diameter of 11 um, corresponding to 697 um^3. Thus, using this average tumor cell size, the mice in Ackerman's study were given an initial a tumor volume of $10{,}455 \times 10^6$ um^3. All cells were assumed to be proliferating initially. The proliferating compartments were divided according to percentages reported in Kumar. Segerstrom et al. reported IMR-32 growth data starting with a tumor volume of 0.46 mL, which thus corresponds to day 20 in our growth model. Ackerman et al. published two sets of IMR-32 growth data. The first set was reported 3 days after tumor inoculation with a tumor size of 17.4 mm^3, corresponding to day 4 in our model. The second set was reported after tumors had reached a mean volume of 182 mm^3, corresponding to day

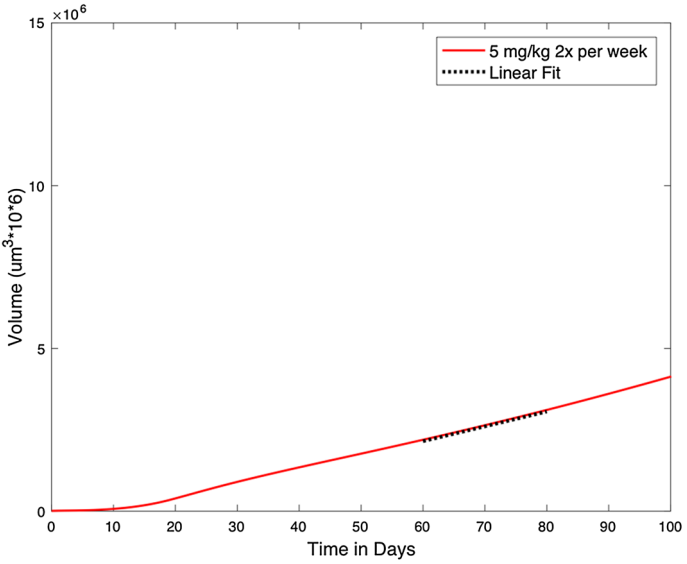

Fig. 2 Growth rate of tumor cells is determined by taking the slope of the linear fit between day 60 and day 80, i.e., the slope of the black dotted segment. The red line indicates predicted tumor volume by our model (Color figure online)

10 in our model. A summary of the spheroid and xenograft growth data can be found in Online Resources 1; parameters for the xenograft model can be found in Table 1.

2.4 Treatment Model

The drug kinetics of bevacizumab can be described by a two-compartment model, with E representing the level of drug in the central compartment, and X representing the level of drug in the peripheral compartment. Pharmacokinetic parameters were given by Wu et al. (2012) (k_{12} (h^{-1}) = 0.0314, k_{21} (h^{-1}) = 0.0131, k_{10} (h^{-1}) = 0.0162).

In the experiment conducted by Segerstrom et al., a bevacizumab treatment regimen of 5 mg/kg twice weekly intraperitoneally was given starting at a tumor size of 0.39 mL, corresponding to the size of the tumor at day 19 in our model. Upon treatment, tumor growth followed a linear growth pattern with a growth rate of 45,807 $um^3 \times 10^{12}$ per day. The growth rate was determined by taking the slope of the linear fit between day 60 and day 80 (shown in black dotted line of Fig. 2). NMRI mice were xenografted at 6 weeks in the experiment done by Segerstrom et al. (2006). A mice body weight of 25 g was used in our xenograft model (Taconic Bioscience 2013). Since, on average, mice have around 58.5 mL of blood per kg of bodyweight, (NC3Rs 2017), a mouse weighing 25 g would therefore have a total blood volume of approximately 58.5 mL/kg $\times$ 0.025 kg = 1.46 mL, giving an initial blood concentration of 85.62 mg/mL corresponding to the experiment in Segerstrom et al.

Drug dosage was incorporated into the model using a step function over a short interval. Parameters c_y and s_y were then determined experimentally to fit the linear regression derived from data.

Table 1 Model parameters are given for monolayer, spheroid, and vascularized xenograft with and without treatment

	Monolayer	Spheroid w/VEGF	Xenograft	Explanation
d_a	0.2	0.2	0.2	Natural death rate
c_1	1.574	1.574	1.574	Transition rate from G_1 to S
c_s	4.4919	4.4919	4.4919	Transition rate from S to G_2
c_2	3.4629	3.4629	3.4629	Transition rate from G_2 to G_1
B	1	Functional response	Functional response	Cells entering Q from G_1
v_0	n/a	3	25*	Nutrient availability
j	n/a	1	1	TNF-a production
k	n/a	0.1	0.1	Rate of TNF-a removal
s_1	n/a	0.1	0.1	Describe functional response B
s_q	n/a	150	150	Describe functional response C
c_v	n/a	0	0.69*	Growth of vasculature
e	n/a	0.45	0.45	Necrotic death of Q
m	n/a	0.01	0.01	Removal of N
s_n	n/a	1000	1000	Describe functional response F
c_q	n/a	18	160*	Describe functional response C
c_f	n/a	0.05	0.05	Apoptosis in proliferating stage due to TNF-a signal
c_R	n/a	n/a	20	VEGF production by proliferating cells
s_R	n/a	n/a	50	TNF-a effect on VEGF production
q_R	n/a	n/a	1	Natural removal of signal due to vasculature
c_{qv}	n/a	n/a	6	Production of VEGF by Q

Table 1 continued

	Monolayer	Spheroid w/VEGF	Xenograft	Explanation
c_{qs}	n/a	n/a	0.48	Describe functional response C
s_v	n/a	n/a	1000	Describe production of VEGF
s_h	n/a	n/a	1	Describe functional response C
f_h	n/a	n/a	1	Describe functional response H
g_h	n/a	n/a	1	Describe functional response H
c_y	n/a	n/a	78**	Removal of VEGF due to therapy
s_y	n/a	n/a	78**	Removal of VEGF due to therapy

*Denotes spheroid parameters that had to be changed in the xenograft model
**Denotes parameters describing treatment by VEGF blocker (Y). Parameters marked n/a are irrelevant to the model output. Initial conditions are in 106 μm^3

2.5 Treatment Experimentation

Bevacizumab is currently approved by the FDA for treatment of metastatic colon cancer, certain lung cancers, renal cancers, ovarian cancers, and glioblastoma multiforme of the brain. In treatment of these cancers, bevacizumab is given 10 mg/kg or 15 mg/kg every 2 week or every 3 weeks via IV bolus (Genentech Inc. 2016). These correspond to 171.23 and 256.85 mg/mL, respectively, in the mice used to build our model (25 g nude mice with total blood volume of 1.46 mL). To maintain consistency with the Segerstrom et al. experiment, treatments in our model were initiated at day 19, when the cell volume was approximately 0.39 mL. This lies within the range of smallest detectable size of tumor of 0.5–4.2 mL (De Bernardi et al. 1992). In addition, various combinations of dosage amount and frequency ranging from 5 to 30 mg/kg and twice a week to once every 3 weeks were given in our model mice for 10.5 weeks, which corresponded to the length of treatment conducted by Segerstrom et al. Goodness of fits in all curves were determined by R^2 values.

2.6 Computational Calculations

All calculations were executed using MATLAB (The Mathworks Inc. 2016). The code is available from the first author.

2.7 Analysis of Equilibrium of System

Theorem *Assuming that all parameters are nonnegative and that the parameters {c_v, v_0, c_R, c_{qv}, j, k, e, m, c_1,} are strictly positive, the system given by Eqs. 1–10 has no equilibria with tumor cells present, i.e., with G_1, S, G_2, Q, or N greater than 0.*

Taking Eq. (8) at equilibrium we have:

$$c_v \frac{R\,(v_0 + V)}{s_v + R + v_0 + V} = 0$$

Under the assumptions above it follows that $R^* = 0$.

Taking Eq. (7) at equilibrium gives:

$$0 = R^{'} = c_R\,(G_2 + S + G_1)\,\frac{A}{s_R + A} + c_{qv}\,Q.$$

since both terms in the expression have nonnegative values, both terms must be zero, giving

$$Q^* = 0 \quad \text{and}$$

$$\text{either} \quad (G_2 + S + G_1) = 0 \quad \text{or } A = 0$$

Thus, two possibilities are considered: (1) in which $Q^* = 0$ and $A^* = 0$, and (2) in which $Q^* = 0$ and $(G_2 + S + G_1)^* = 0$.

Case I: $\boldsymbol{Q^* = 0}$ and $\boldsymbol{A^* = 0}$.

Taking Eq. (6) at equilibrium gives:

$$A' = jN - k\,(v_0 + V)\,A = 0$$

From which it follows that $N^* = 0$.

Taking Eq. (5) at equilibrium gives:

$$N' = eHQ - m\,(v_0 + V)\,N = 0$$

From which it follows that $Q^* = 0$.

Proceeding in a similar fashion, taking Eq. (4) at equilibrium gives $G_1{}^* = 0$.

Summing Eqs. (1–3) at equilibrium gives $(G_1 + S + G_2)' = 0$, or

$$c_2 G_2 - c_1\,(1 - B)\,G_1 - c_f \frac{A}{s_n + A}(G_2 + S + G_1) + CQ - d_a G_2 = 0.$$

Using that $G_1{}^*$, A^*, and Q^* are all 0 gives

$$c_2 G_2 - d_a G_2 = 0$$

and therefore

$$\boldsymbol{G}_2^* = \mathbf{0}.$$

Equation (2) then implies that $S^* = 0$ at equilibrium:

Thus, at equilibrium, $G_1{}^* = 0$, $S^* = 0$, $G_2{}^* = 0$, $Q^* = 0$, and $N^* = 0$.

Case II: $\boldsymbol{Q}^* = \mathbf{0}$ and $(\boldsymbol{G}_2 + \boldsymbol{S} + \boldsymbol{G}_1)^* = \mathbf{0}$:

As all quantities are nonnegative it suffices to show that $N^* = 0$.

Taking Eq. (5) at equilibrium:

$$N' = eHQ - m(v_0 + V)N = 0$$

from which we conclude that $N^* = 0$.q.e.d.

Corollary *Under the same assumptions as the theorem and assuming {j, k, c_v} are positive, $R^* = 0$ and $A^* = 0$.*

The proof follows easily from Eqs. (6) and (8).

Thus, many equilibria exist depending on the level of vasculature. That is, V^* may be anything at equilibrium. In each equilibrium, however, tumor cell populations are zero.

2.8 Analysis of Stability at the Equilibrium $P = Q = N = R = A = V = 0$

Note that in Eqs. (1)–(10) the variable quantity V always occurs as part of the expression $(v_0 + V)$. Thus, whatever V^* may be can be included as part of the existing pre-angiogenic vasculature v_0. So, without loss of generality, we can take $V = 0$. The Jacobian matrix of the model at this equilibrium is given by:

$$J = \begin{bmatrix}
-c_1 & \frac{c_1 v_0}{s_1 + v_0} & 0 & c_1 - \frac{c_1 v_0}{s_1 + v_0} & 0 & 0 & 0 & 0 \\
0 & -c_s & c_s & 0 & 0 & 0 & 0 & 0 \\
2c_2 & 0 & -c_2 - d_a & 0 & 0 & 0 & 0 & 0 \\
0 & \frac{c_q v_0}{s_q + v_0} & 0 & \frac{-c_q v_0}{s_q + v_0} - e & e & 0 & c_{qv} & 0 \\
0 & 0 & 0 & 0 & -m v_0 & j & 0 & 0 \\
0 & 0 & 0 & 0 & 0 & -k v_0 & 0 & 0 \\
0 & 0 & 0 & 0 & 0 & 0 & -p_R v_0 & \frac{c_v v_0}{c_v + v_0} \\
0 & 0 & 0 & 0 & 0 & 0 & 0 & 0
\end{bmatrix}$$

As the Jacobian is block diagonal, its roots are given by the roots of a quartic determined by the 4 by 4 upper left block, and the easily identified roots of the lower right block. However, the roots of the quartic are not easily determined in general, so for this case, the eigenvalues were determined using the software R 3.3.1 (R Development Core Team 2011). The sign of the real part of at least one eigenvalue was positive, indicating an unstable equilibrium (eigenvalues: -25.00, -23.32, $-5.18 + 3.01$i, $-5.18 - 3.01$i, -2.50, 0.64, -0.25, and 0.00).

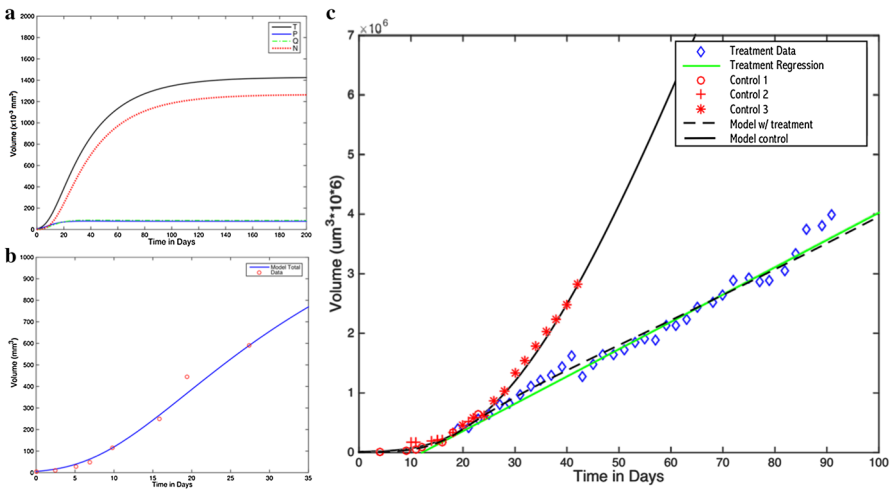

Fig. 3 Verification of model. **a** Our model reproduced a known spheroid tumor growth dynamic: regardless of initial conditions of the spheroid tumor, it eventually reach equilibrium with three layers of proliferating, quiescent, and necrotic cells. **b** The spheroid model matched experimental spheroid growth data. The spheroid system was reproduced by setting v_0 to zero. **c** The full xenograft model fits experimental data with and without bevacizumab treatment. Treatment regimen was 5 mg/kg twice a week. Tumor volume after treatment was fit with linear regression line (green). Control 1 and control 2 growth data were both extracted from Ackerman et al. Control 3 growth data and treatment growth data were extracted from Segerstrom et al (Color figure online)

3 Results

3.1 Our Model can Accurately and Precisely Predict Tumor Growth In Vitro and In Vivo with and Without Treatment

Our model is able to accurately replicate several sets of experimental growth data of IMR-32 as a monolayer, spheroid, and xenograft with and without bevacizumab treatment. The nested structure of the model allows it to address three very different types of experimental data, with parameters tuned specifically to each experiment.

The monolayer model was able to produce a tumor cell that, after 2 days, had a cell cycle distribution of G_1, S, and G_2 and percent death similar to those reported by Kumar et al. (2014). When extended to include quiescent and necrotic cells and TNF-alpha, the spheroid model could match spheroid growth data (Fig. 3b) (Carlsson et al. 1983) and final size of the necrotic core. It was also able to replicate a key phenomenon observed in spheroid growth: no matter what the initial conditions, eventually reach equilibrium with three layers of proliferating, quiescent, and necrotic cells (Sherar et al. 1987; Folkman et al. 1966) (Fig. 3a). In addition, Folkman noted that tumors could not grow beyond a diameter of three to four millimeters (volume of 1.4×10^{10} um^3), regardless of how often new medium is provided or how much space is made available (Folkman 1974; Folkman et al. 1966). Our spheroid model replicates a similar growth phenomenon, with total tumor size reaching an equilibrium of approximately 1.4×10^9 um^3 (Fig. 3a).

The xenograft model was able to replicate Ackerman et al. and Segerstrom et al. experimental data with and without bevacizumab treatment (Fig. 3c) (Ackermann et al. 2011; Segerström et al. 2006). Furthermore, regardless of whether treatment was given in the xenograft model, the tumor eventually reached a linear growth rate, consistent with previous results on the universal dynamics of tumor grow (Brú et al. 2003) (Fig. 3c).

Many experiments have reported decreased plasma VEGF level and tumor growth upon cells receiving various anti-VEGF treatments, including the drug of interest, bevacizumab (Segerström et al. 2006; Bäckman and Christofferson 2005; Keating 2014; Hurwitz et al. 2005). In our model, when bevacizumab treatment is implemented in the xenograft model, VEGF levels, vasculature levels, and total tumor size are diminished, thus further confirming the validity of our model. More specifically, though Segerstrom et al. do not report the results of plasma VEGF levels after treatment, our model indicates a 67% drop in VEGF levels after 10.5 weeks of treatment (Fig. 4a).

3.2 VEGF Levels Demonstrates a Linear Relationship with Vasculature Levels and Total Tumor Size

One key characteristic of our model is its ability to quantify vascularization of the tumor. While the units of vasculature in our model are arbitrary, the values prove to be useful in comparisons and correlational studies. It is well established that VEGF promotes tumor angiogenesis; Hicklin and Lee et al. both concluded that VEGF promotes tumor angiogenesis and that anti-VEGF receptors suppress tumor growth (Hicklin and Ellis 2005; Lee et al. 2015). However, no clear relationship between the two has been established in the past. By comparing the VEGF levels to vasculature and total tumor size at after 10.5 weeks of growth with and without treatment, we can conclude that there is a direct proportional relationship between VEGF and vascularization (Fig. 4b).

3.3 Total Administered Bevacizumab Concentration, as Opposed to Dosage Regimen, is the Major Determining Factor in Tumor Suppression Ability of Drug

Bevacizumab is the first angiogenesis inhibitor proven to be effective in delaying tumor progression in patients with various cancers (Keating 2014). Backman et al. showed that bevacizumab significantly inhibits VEGF production in neuroblastoma growth, and the results from Segerstrom et al. indicate that a treatment regimen of 5 mg/kg bevacizumab twice a week is sufficient to significantly decrease neuroblastoma growth in mice (Segerström et al. 2006; Bäckman and Christofferson 2005). The dose of bevacizumab given in Segerstrom's study was identical to those given in patients in Hurwitz's study (Hurwitz et al. 2005) but with a shorter interval, twice weekly compared to every second week. Though it is logical to assume that higher dosage and increased frequency of bevacizumab treatment lead to greater tumor growth suppression, the relationship has not been clearly established in the literature. Our results indicate that there is no significant difference in growth rate inhibition between

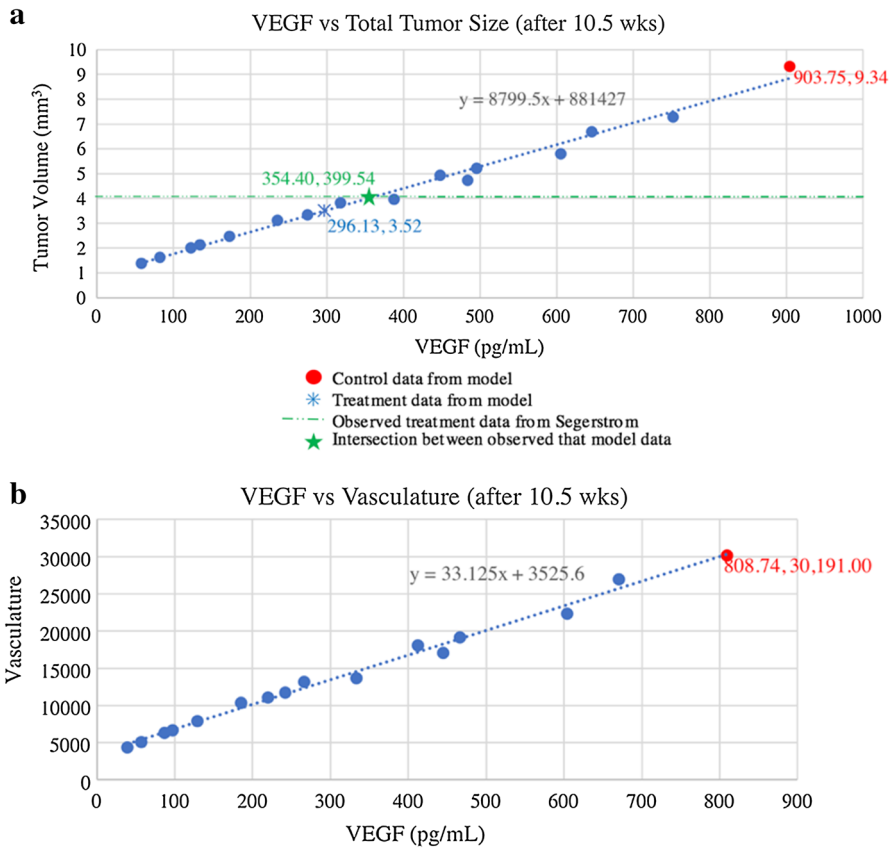

Fig. 4 Our model was able to predict VEGF and vasculature of the xenograft tumor. **a** VEGF levels were plotted against the tumor size after 10.5 weeks with and without treatment. The red dot data point represents data from Segerstrom et al. without treatment after 10.5 weeks. The green dashed line represents the reported data from Segerstrom et al. after 5 mg/kg bevacizumab was given twice a week for 10.5 weeks. The blue star is the predicted tumor size and VEGF levels after 5 mg/kg bevacizumab twice a week for 10.5 weeks in the model mice. **b** VEGF levels were plotted against vasculature after 10.5 weeks. The red data point represents data from Segerstrom et al. without treatment after 10.5 weeks (Color figure online)

model mice given an entire dose at once compared to mice given the same amount of drug but divided up over several days. For example, implementing 10 mg/kg once a week inhibited IMR-32 tumor growth rate in the model mice to the same extent as a treatment consisting of 5 mg/kg twice a week and 20 mg/kg once every other week (Fig. 5a).

3.4 There is an Exponentially Decreasing Relationship Between the Bevacizumab Levels In Vivo and the Growth Rate of IMR-32

While Segerstrom et al. suggested in their discussion that increasing the dose will not affect the anti-tumor activity due to the long half-life of drug, our results indicate

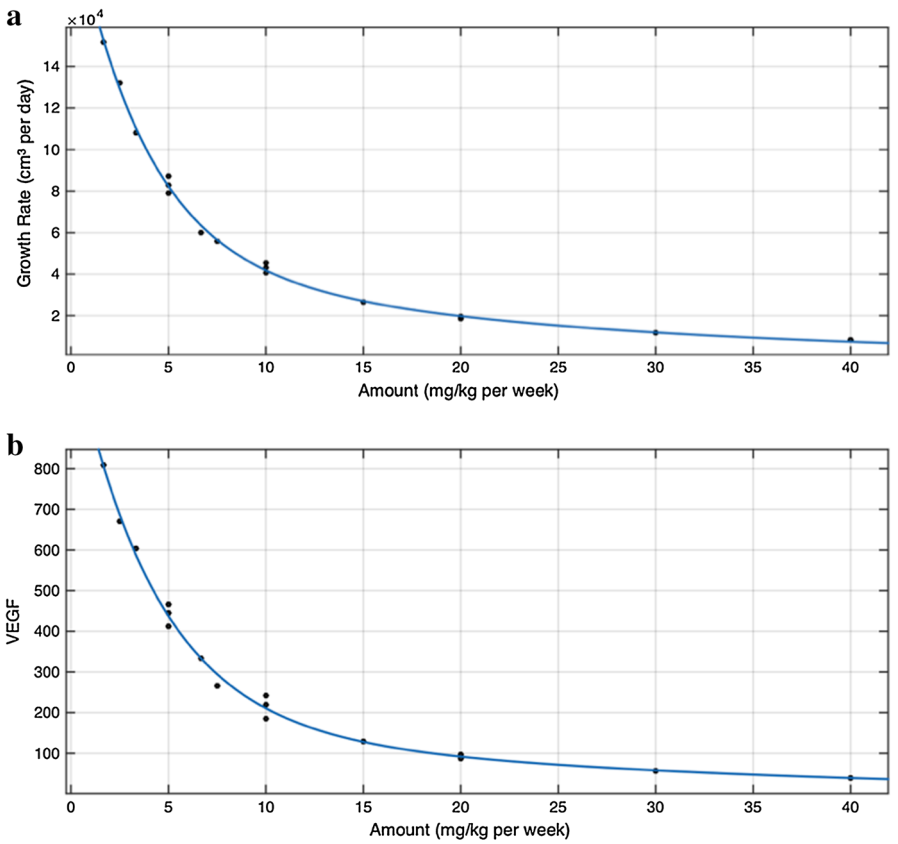

Fig. 5 Various bevacizumab treatment regimens were tests on the model, and the growth rate was determined for each trial. The x axis represents total amount of bevacizumab given per week. There is an exponentially decreasing relationship between the bevacizumab levels and the growth rate (**a**) and VEGF production (**b**). Treatments with the same total amount per week but different regimens show roughly the same inhibition of growth rate (**a**) and VEGF production (**b**)

otherwise. Our results predict an exponentially decreasing relationship between the total drug amount in the body and the growth rate (Fig. 5a).

4 Discussion

We have shown a simple but complete compartmental model that describes xenograft in vivo growth of IMR-32 neuroblastoma with and without anticancer drug bevacizumab treatment. The model is built upon a previously published spheroid model but now takes into consideration angiogenesis, which gives tumors the distinct ability to grow and metastasize by providing vascularization. More specifically, vascular endothelial growth factor (VEGF), a highly expressed tumor angiogenesis factor that promotes vascularization in tumors, is incorporated into the model via functions that relate to cells of all three states of the tumor: the proliferating compartments (G_2

$+S+G_2$), the necrotic compartment (N), and the hypoxic quiescent compartment (Q). Despite these complex processes, the model consisted of approximately as many parameters as there are measured quantities, making it an attractive and accessible tool to further understand tumor growth dynamics.

Our model was parameterized using the results of several published experiments with and without treatment. It was able to not only match all sets of xenograft total tumor size data, but also predict monolayer cell cycle dynamics and spheroid growth data accurately by turning off vasculature (spheroid model) or also turning off G_1 to Q transition (monolayer model). In addition, it replicates a key observation of the dynamics of spheroid tumor growth: the sphere will eventually reach an equilibrium total tumor size with three stable layers of proliferating, quiescent, and necrotic cells (Sherar et al. 1987; Folkman et al. 1966). Furthermore, regardless of control or drug treatments, the tumor eventually reach a linear growth rate, consistent with previous observations on the universal dynamics of vascularized tumor grow (Brú et al. 2003).

Few methods of quantifying vasculature experimentally exist. One such procedure requires knowledge of many parameters, many of which can be difficult to obtain experimentally (Wassberg et al. 1999). Our model is able to easily and quickly quantify vascularization of the tumor. Although the units of vasculature in our model are arbitrary, the values prove to be useful in comparisons and correlational studies. The capacity of our model to quantify VEGF production gave us key insights into tumor growth dynamics. Most notably, there is a direct proportional relationship between VEGF and vascularization as well as between VEGF and total tumor size (Fig. 4).

Bevacizumab is first angiogenesis inhibitor proven to be effective in delaying tumor progression in patients with various cancer and is now commonly used for treatment of various cancers (Keating 2014). Backman et al. showed that bevacizumab significantly inhibits VEGF production in neuroblastoma growth, and the results from Segerstrom et al. indicate that a treatment regimen of 5 mg/kg bevacizumab twice a week is sufficient to significantly decrease neuroblastoma growth in mice. Though Segerstrom do not report the results of plasma VEGF levels after treatment, our model indicates a 67% drop in VEGF levels after 10.5 weeks of treatment (Fig. 5). These results are supported by other studies that have shown a decreased plasma VEGF level after anti-VEGF drug treatment (Bäckman and Christofferson 2005).

Furthermore, our results indicate that the total amount of drug is more important in determining the ability of the drug to inhibit growth rate, rather than treatment regimen. This suggests that, if only tumor growth suppression ability is considered, there is no advantage to administering the drug in smaller and more frequent doses rather than one large dose. Of course, in a clinical setting, other factors, such as potential side effects of the drug, must be considered in determining treatment regimens.

Our model established a decreasing exponential relationship between the amount of bevacizumab administered to the model mice and the neuroblastoma growth rate. This provides a valuable insight into the effect of bevacizumab on neuroblastoma: It suggests a limited range in which increasing the drug level will continue to significantly reduce the neuroblastoma growth rate.

While bevacizumab was effective in slowing down the growth rate of neuroblastoma, it failed to kill off the tumor. Previous research indicates that there are synergistic effects when a VEGF inhibitor drug and a cytotoxic drug are combined in treatment

(Lv et al. 2013; Sweeney et al. 2003; Gerber and Ferrara 2005). Further testing is needed with our model to determine the optimal multidrug combination treatment for neuroblastoma. Our model is versatile enough to add additional compartments for cytotoxic drugs.

In conclusion, we have presented a simple compartmental mathematical model that is able to fit both qualitative and quantitative observations of xenograft growth in vivo with and without treatment. The model provides direct quantitative insight into VEGF and vasculature levels of the tumor at all stage of developments. We conclude that bevacizumab dosage has a negative exponential relationship with both the growth rate and VEGF levels. Furthermore, our results suggest no significant difference in tumor growth suppression ability between a single large bevacizumab dose compared to separating treatment into more frequent doses of smaller concentration.

Acknowledgements This work was supported by the Women in Science Program, Sophomore Science Scholars Program, James O. Freedman Presidential Scholar, and Undergraduate Leave Term Research Grant to Yixuan He from the Office of Undergraduate Research at Dartmouth College.

References

Ackermann S, Goeser F, Schulte JH, Schramm A, Ehemann V, Hero B, Eggert A, Berthold F, Fischer M (2011) Polo-like kinase 1 is a therapeutic target in high-risk neuroblastoma. Clin Cancer Res 17(4):731–741. https://doi.org/10.1158/1078-0432.CCR-10-1129

Alarcon T, Byrne H, Maini P, Panovska J (2005) 20 Mathematical modelling of angiogenesis and vascular adaptation. Stud Multidiscip 3(C):369–387. https://doi.org/10.1016/s1571-0831(06)80024-9

Alarcón T, Owen MR, Byrne HM, Maini PK (2006) Multiscale modelling of tumour growth and therapy: the influence of vessel normalisation on chemotherapy. Comput Math Methods Med. https://doi.org/10.1080/10273660600968994

Argyri KD, Dionysiou DD, Misichroni FD, Stamatakos GS (2016) Numerical simulation of vascular tumour growth under antiangiogenic treatment: addressing the paradigm of single-agent bevacizumab therapy with the use of experimental data. Biol Direct 11(1):12. https://doi.org/10.1186/s13062-016-0114-9

Bäckman U, Christofferson R (2005) The selective class III/V receptor tyrosine kinase inhibitor SU11657 inhibits tumor growth and angiogenesis in experimental neuroblastomas grown in mice. Pediatr Res 57(5 I):690–695. https://doi.org/10.1203/01.pdr.0000156508.68065.aa

Botchkina GI, Meistrell ME, Botchkina IL, Tracey KJ (1997) Expression of TNF and TNF receptors (p55 and p75) in the rat brain after focal cerebral ischemia. Mol Med 3(11):765–781. http://www.ncbi.nlm.nih.gov/pmc/articles/PMC2230243/

Brú A, Albertos S, Subiza JL, García-Asenjo JL, Brú I (2003) The universal dynamics of tumor growth. Biophys J 85(November):2948–2961. https://doi.org/10.1016/S0006-3495(03)74715-8

Byrne HM (2010) Dissecting cancer through mathematics: from the cell to the animal model. Nat Rev Cancer 10(3):221–230. https://doi.org/10.1038/nrc2808

Carlsson J, Nilsson K, Westermark B, Pontén J, Sundström C, Larsson E, Bergh J, Påhlman S, Busch C, Collins VP (1983) Formation and growth of multicellular spheroids of human origin. Int J Cancer 31(5):523–533. https://doi.org/10.1002/ijc.2910310502

De Bernardi B, Pianca C, Boni L, Brisigotti M, Carli M, Bagnulo S, Corciulo P, Mancini A, De Laurentis C, Di Tullio MT (1992) Disseminated neuroblastoma (stage IV and IV-S) in the first year of life. Outcome related to age and stage. Italian Cooperative group on neuroblastoma. Cancer 70(6):1625–1633

De Mattei V, Flandoli F, Leocata M, Polito MC, Ricci C (2016) A mathematical model for growth of solid tumors and combination therapy with an application to colorectal cancer, 1–21. http://arxiv.org/abs/1607.08009

Demidenko E (2006) The assessment of tumour response to treatment. J R Stat Soc Ser C (Appl Stat) 55(3):365–377. http://www.jstor.org.dartmouth.idm.oclc.org/stable/4126391

Edmondson R, Broglie JJ, Adcock AF, Yang L (2014) Three-dimensional cell culture systems and their applications in drug discovery and cell-based biosensors. Assay Drug Dev Technol 12(4):207–218. https://doi.org/10.1089/adt.2014.573

Folkman J (1974) Tumor angiogenesis 11 this work was supported by a grant from the National Cancer Institute (No. 1 RO1 CA 14019–01), a grant from the American Cancer Society (No. DT-2A), and gifts from Alza Corporation, Merck Co., and Mr. Morton Bank. Adv Cancer Res 19:331–358. https://doi.org/10.1016/S0065-230X(08)60058-5

Folkman J, Hochberg M (1973) Self-regulation of growth in three dimensions. J Exp Med 138(4):745–753. http://www.ncbi.nlm.nih.gov/pmc/articles/PMC2180571/

Folkman J, Cole P, Zimmerman S (1966) Tumor behavior in isolated perfused organs: in vitro growth and metastases of biopsy material in rabbit thyroid and canine intestinal segment. Ann Surg 164(3):491–502. http://www.ncbi.nlm.nih.gov/pmc/articles/PMC1477290/

Freyer P (1988) Role of necrosis in regulating the growth saturation of multicellular spheroids. Cancer Res 48(9):2432–2439

Genentech Inc. (2017) Avastin prescribing information. Genentech, Inc.

Gerber H-P, Ferrara N (2005) Pharmacology and pharmacodynamics of bevacizumab as monotherapy or in combination with cytotoxic therapy in preclinical studies. Cancer Res 65(3):671–680

Hahnfeldt P, Panigrahy D, Folkman J, Hlatky L (1999) Tumor development under angiogenic signaling: a dynamical theory of tumor growth, treatment response, and postvascular dormancy. Cancer Res 59(19):4770–4775

Hicklin DJ, Ellis LM (2005) Role of the vascular endothelial growth factor pathway in tumor growth and angiogenesis. J Clin Oncol Off J Am Soc Clin Oncol 23(5):1011–1027. https://doi.org/10.1200/jco.2005.06.081

Hurwitz HI, Fehrenbacher L, Hainsworth JD, Heim W, Berlin J, Holmgren E, Hambleton J, Novotny WF, Kabbinavar F (2005) Bevacizumab in combination with fluorouracil and leucovorin: an active regimen for first-line metastatic colorectal cancer. J Clin Oncol Off J Am Soc Clin Oncol 23(15):3502–3508. https://doi.org/10.1200/jco.2005.10.017

Jing Y, Ma N, Fan T, Wang C, Xinxin B, Jiang G, Li R et al (2011) Tumor necrosis factor-alpha promotes tumor growth by inducing vascular endothelial growth factor. Cancer Investig 29(7):485–493. https://doi.org/10.3109/07357907.2011.597812

Keating GM (2014) Bevacizumab: a review of its use in advanced cancer. Drugs 74(16):1891–1925. https://doi.org/10.1007/s40265-014-0302-9

Kim JB (2005) Three-dimensional tissue culture models in cancer biology. Semin Cancer Biol 15(5):365–377. https://doi.org/10.1016/j.semcancer.2005.05.002

Kumar A, Fan D, DiPette DJ, Singh US (2014) Sparstolonin B, a novel plant derived compound, arrests cell cycle and induces apoptosis in N-myc amplified and N-myc nonamplified neuroblastoma cells. PLoS ONE 9(5):e96343. https://doi.org/10.1371/journal.pone.0096343

Landry J, Freyer JP, Sutherland RM (1982) A model for the growth of multicellular spheroids. Cell Tissue Kinet 15(6):585–594

Lee SH, Jeong D, Han Y-S, Baek MJ (2015) Pivotal role of vascular endothelial growth factor pathway in tumor angiogenesis. Ann Surg Treat Res. https://doi.org/10.4174/astr.2015.89.1.1

Leeuwenberg JFM, van Tits LJH, Jeunhomme TMAA, Buurman WA (1995) Evidence for exclusive role in signalling of tumour necrosis factor p55 receptor and a potentiating function of p75 receptor on human endothelial cells. Cytokine 7(5):457–462. https://doi.org/10.1006/cyto.1995.0062

Lignet F, Benzekry S, Wilson S, Billy F, Saut O, Tod M, You B et al (2013) Theoretical investigation of the efficacy of antiangiogenic drugs combined to chemotherapy in xenografted mice. J Theor Biol 320(March):86–99. https://doi.org/10.1016/j.jtbi.2012.12.013

Lu J-F, Bruno R, Eppler S, Novotny W, Lum B, Gaudreault J (2008a) Clinical pharmacokinetics of bevacizumab in patients with solid tumors. Cancer Chemother Pharmacol. https://doi.org/10.1007/s00280-007-0664-8

Lu J-F, Bruno R, Eppler S, Novotny W, Lum B, Gaudreault J (2008b) Clinical pharmacokinetics of bevacizumab in patients with solid tumors. Cancer Chemother Pharmacol 62(5):779–786. https://doi.org/10.1007/s00280-007-0664-8

Lv C, Shuodong W, Zheng D, Yuli W, Yao D, Xiaopeng Yu (2013) The efficacy of additional bevacizumab to cytotoxic chemotherapy regimens for the treatment of colorectal cancer: an updated meta-analysis for randomized trials. Cancer Biother Radiopharm 28(7):501–509. https://doi.org/10.1089/cbr.2012.1458

Marušić M, Bajzer Ž, Freyer JP, Vuk-Pavlović S (1994) Analysis of growth of multicellular tumour spheroids by mathematical models. Cell Prolif 27(2):73–94. https://doi.org/10.1111/j.1365-2184.1994.tb01407.x

Menchón SA, Condat CA (2008) Cancer growth: predictions of a realistic model. Phys Rev E Stat Nonlinear Soft Matter Phys 78(2 Pt 1):22901. https://doi.org/10.1103/physreve.78.022901

Menchón SA, Condat CA (2009) Modeling tumor cell shedding. Eur Biophys J 38(4):479–485. https://doi.org/10.1007/s00249-008-0398-5

Mollard S, Ciccolini J, Imbs D-C, El Cheikh R, Barbolosi D, Benzekry S (2017) Model driven optimization of antiangiogenics + cytotoxics combination: application to breast cancer mice treated with bevacizumab + paclitaxel doublet leads to reduced tumor growth and fewer metastasis. Oncotarget 8(14):23087–23098. https://doi.org/10.18632/oncotarget.15484

NC3Rs (2017) Mouse: decision tree for blood sampling | NC3Rs. https://www.nc3rs.org.uk/mouse-decision-tree-blood-sampling. Accessed 1 Jan 2017

Piantadosi S (1985) A model of growth with first-order birth and death rates. Comput Biomed Res Int J 18(3):220–232

Pinho STR, Bacelar FS, Andrade RFS, Freedman HI (2013) A mathematical model for the effect of anti-angiogenic therapy in the treatment of cancer tumours by chemotherapy. Nonlinear Anal Real World Appl 14(1):815–828. https://doi.org/10.1016/j.nonrwa.2012.07.034

Poleszczuk J, Hahnfeldt P, Enderling H (2015) Therapeutic implications from sensitivity analysis of tumor angiogenesis models. PLoS ONE 10(3):e0120007. https://doi.org/10.1371/journal.pone.0120007

R Development Core Team (2011) R: a language and environment for statistical computing, vol 1. R Foundation for Statistical Computing, Vienna. https://doi.org/10.1007/978-3-540-74686-7

Sasi SP, Yan X, Enderling H, Park D, Gilbert H-Y, Curry C, Coleman C et al (2012) Breaking the 'harmony' of TNF-alpha signaling for cancer Treatment. Oncogene 31(37):4117–4127. https://doi.org/10.1038/onc.2011.567

Seeger RC, Rayner SA, Banerjee A, Benedict WF, Chung H, Laug WE, Neustein HB (1977) Morphology, growth, chromosomal pattern, and fibrinolytic activity of two new human neuroblastoma cell lines. Cancer Res 37(5):1364–1371

Segerström L, Fuchs D, Bäckman U, Holmquist K, Christofferson R, Azarbayjani F (2006) The anti-VEGF antibody bevacizumab potently reduces the growth rate of high-risk neuroblastoma xenografts. Pediatr Res 60(5):576–581. https://doi.org/10.1203/01.pdr.0000242494.94000.52

Sherar MD, Noss MB, Foster FS (1987) Ultrasound backscatter microscopy images the internal structure of living tumour spheroids. Nature 330(6147):493–495. https://doi.org/10.1038/330493a0

Shweiki D, Itin A, Soffer D, Keshet E (1992) Vascular endothelial growth factor induced by hypoxia may mediate hypoxia-initiated angiogenesis. Nature 359(6398):843–845. https://doi.org/10.1038/359843a0

Sims TL, Williams RF, Ng CY, Rosati SF, Spence Y, Davidoff AM (2008) Bevacizumab suppresses neuroblastoma progression in the setting of minimal disease. Surgery 144(2):269–275. https://doi.org/10.1016/j.surg.2008.04.009

Sweeney CJ, Miller KD, Sledge GW Jr (2003) Resistance in the anti-angiogenic era: nay-saying or a word of caution? Trends Mol Med 9(1):24–29

Szlosarek PW, Balkwill FR (2003) Tumour necrosis factor [alpha]: a potential target for the therapy of solid tumours. Lancet Oncol 4(9):565

Taconic Bioscience (2013) NCr nude mice | athymic mouse model. https://www.taconic.com/mouse-model/ncr-nude

Takagi A, Watanabe M, Ishii Y, Morita J, Hirokawa Y, Matsuzaki T, Shiraishi T (2007) Three-dimensional cellular spheroid formation provides human prostate tumor cells with tissue-like features. Anticancer Res 27(1A):45–53

Tan PH, Chan C, Xue SA, Dong R, Ananthesayanan B, Manunta M, Kerouedan C et al (2004) Phenotypic and functional differences between human saphenous vein (HSVEC) and umbilical vein (HUVEC) endothelial cells. Atherosclerosis 173(2):171–183. https://doi.org/10.1016/j.atherosclerosis.2003.12.011

Tang L, Van De Ven AL, Guo D, Andasari V, Cristini V, Li KC, Zhou X (2014) Computational modeling of 3D tumor growth and angiogenesis for chemotherapy evaluation. PLoS ONE 9(1):1–12. https://doi.org/10.1371/journal.pone.0083962

The Mathworks Inc. (2016) MATLAB—mathworks. www.mathworks.com/products/matlab. doi: 2016-11-26

U.S. Cancer Statistics Working (2017) United States cancer statistics: 1999–2014 incidence and mortality web-based report. *Atlanta: U.S. Department of Health and Human Services, Centers for Disease Control and Prevention and National Cancer Institute*, no. 888: 6348. www.cdc.gov/uscs

Wallace DI, Guo X (2013) Properties of tumor spheroid growth exhibited by simple mathematical models. Front Oncol 3(March):51. https://doi.org/10.3389/fonc.2013.00051

Wallace DI, Dunham A, Chen PX, Chen M, Huynh M, Rheingold E, Prosper O (2016) A model for spheroid versus monolayer response of SK-N-SH neuroblastoma cells to treatment with 15-deoxy-PGJ 2. Comput Math Methods Med 2016:1–11. https://doi.org/10.1155/2016/3628124

Wassberg E, Hedborg F, Sköldenberg E, Stridsberg M, Christofferson R (1999) Inhibition of angiogenesis induces chromaffin differentiation and apoptosis in neuroblastoma. Am J Pathol 154(2):395–403. https://doi.org/10.1016/S0002-9440(10)65286-8

Wu F, Tamhane M, Morris M (2012) Pharmacokinetics, lymph node uptake, and mechanistic PK model of near-infrared dye-labeled bevacizumab after IV and SC administration in mice. AAPS J 14(2):252–261. https://doi.org/10.1208/s12248-012-9342-9